
Directional aspects of vegetation linear and circular polarization biosignatures

C.H. Lucas Patty^{1*}, Antoine Pommerol¹, Jonas G. Kühn^{2,3}, Brice-Olivier Demory², Nicolas Thomas¹

¹ Physikalisches Institut, Universität Bern, CH-3012 Bern, Switzerland

² Center for Space and Habitability, Universität Bern, CH-3012 Bern, Switzerland

³ Département d'Astronomie, Université de Genève, CH-1290 Versoix, Switzerland

*lucas.patty@unibe.ch, chlucaspatty@gmail.com

Abstract

Homochirality is a generic and unique property of all biochemical life and is considered a universal and agnostic biosignature. Upon interaction with unpolarized light, homochirality induces fractional circular polarization in the light that is scattered from it, which can be sensed remotely. As such, it can be a prime candidate biosignature in the context of future life-detection missions and observatories. The linear polarizance of vegetation is also sometimes envisaged as a biosignature, although it does not share the molecular origin as circular polarization. It is known that the linear polarization of surfaces is strongly dependent on the phase angle. The relation between the phase angle and circular polarization stemming from macromolecular assemblies, such as in vegetation, however, remained unclear. We demonstrate in this study using the average of 27 different species that the circular polarization phase angle dependency of vegetation induces relatively small changes in spectral shape and mostly

affects the signal magnitude. With these results we underline the use of circular spectropolarimetry as a promising agnostic biosignature complementary to the use of linear spectropolarimetry and scalar reflectance.

Spectropolarimetry, Biosignatures, Remote Sensing, Homochirality, Photosynthesis, Life Detection

1 Introduction

While in recent decades the use of polarimetry for aerosol particle and cloud characterization has rapidly been established, optical remote sensing of surfaces using polarimetry is not broadly established. Instrumentation for the acquisition of sensitive linear polarimetry has matured towards the point that they can be readily applied for such purposes. Interpretation of the linear polarizance, however, is difficult especially due to the strong phase angle dependency.

In recent years, circular spectropolarimetric instruments have also been developed allowing the sensitive acquisition of circular polarization of vegetation in the field [1] and from a swift moving helicopter [2]. The circular polarizance by biopigments provides a unique spectropolarimetric biosignature and is generally absent in the light scattered of abiotic surfaces [1–3]. While abiotic materials can also create circular polarization, such as through multiple scattering by clouds or aerosols, these interactions result in a weaker and spectrally flat circular polarization signal [4]. Rather than being the result of surface scattering, the circular polarizance of photosynthetic organisms, including algae and bacteria, primarily results from interactions with chiral pigment-protein complexes inside the cells [5–7].

Terrestrial biochemistry is based on chiral molecules which determine both the functioning and structure of biological systems. Unlike abiotic chemistry, where these molecules occur in equal, racemic, concentrations of both versions,

living nature almost [8] exclusively utilizes these molecules in only one of the mirror image configurations (homochirality). Biological macromolecules and biomolecular architectures are often also homochiral. The α -helix, for example, the most prevalent secondary structure of proteins, is almost [9] exclusively right-hand-coiled. Homochirality is a prerequisite for self-replication and thus for life as we know it [10–12]. It is likely that homochirality is a universal feature of life [3, 5, 13, 14] and may serve as an agnostic trait of life itself. Nonetheless, a lack of homochirality does not necessarily indicate an absence of life and false-negative scenarios can be possible [15].

The chirality of molecules and molecular architectures endows them a specific response to electromagnetic radiation [5, 16]. When unpolarized incident light, such as emitted from the Sun [17], is reflected off a homochiral material it induces a wavelength dependent fractional circular polarization signal, which can thus be detected remotely. It has been demonstrated that the circular polarizance of vegetation carries the same information as circular dichroism [18, 19], which is the differential absorbance of left- and right-handed circularly polarized incident light, and has proven to be an indispensable tool in biomolecular research.

In vegetation, the chlorophylls are organized in chiral protein-pigment aggregates. It is the chirality of the supramolecular structure, that dominates the circular polarization spectrum rather than the chirality of the constituent molecules themselves. While the signals resulting from smaller scale chirality are superimposed, the total polarization spectrum is not the sum of these spectra alone [20, 21]. These supramolecular chiral aggregates can create very intense polarization signals (polymer and salt induced (psi-type) polarization) that can be up to two orders of magnitude larger than the polarization of the constituents. Additionally, psi-type polarization is characterized by non-conservative anomalously shaped bands that range beyond the wavelengths of molecular ab-

sorbance. Due to the direct relation between the circular polarizance and the macromolecular structure it is an highly sensitive indicator of the membrane macro-organization of the photosynthetic apparatus and its functioning [22, 23].

As such, vegetation circular polarizance could provide sensitive monitoring of vegetation physiology [24]. It has been demonstrated that circular polarization can be very indicative of stress factors such as drought and can in principle also be used to detect different physiological stress responses [18, 24]. While vegetation circular polarizance is typically less than 1%, making its use challenging for instrumentation, polarization remote sensing could prove to be a very powerful complementary tool in assessing climate change, desertification, deforestation and the general monitoring of vegetation physiological state in vulnerable regions [2].

Additionally, also linear dichroism spectroscopy has contributed significantly to the understanding of molecular organization. In principle, linear polarizance would yield the same results as linear dichroism. However, the retrieval of structural information through linear spectropolarimetry is dependent on the molecular alignment of the sample. In a randomly oriented sample this information is therefore averaged out, even if the sample possesses intrinsically anisotropic molecular architectures [22, 23]. The linearly polarized proportion of the light reflected of vegetation generally stems from leaf surface polarization and the light scattered by leaf internal structures is only polarized to a small extent [25, 26]. As such, linear polarizance will not carry any information on molecular arrangements. It has however been demonstrated that remote sensing using linear polarization can be informative of plant physiological status [27–29], and can aid in estimating leaf chlorophyll content [30]. The linear polarizance of vegetation can be a sensitive biosignature [31, 32] that can be complementary to the scalar reflectance and circular polarizance.

Beside leaf optical properties such as the optical index of refraction from the cuticle and/or epidermis and the surface roughness, the linear polarizance of leaves is highly dependent on the angle of the incident light [25, 33]. This is largely due to the increase in specular reflection by the leaf surface as a function of the angle of incidence [34]. This effect becomes stronger in the pigment absorption bands, where the main contribution to the total reflection comes from the specular reflectance on the surface and the scattered light by the leaf internal structures will be absorbed. Reciprocally, the linear polarizance is lowest in the near-infrared, where no significant absorption occurs and the contribution of internally scattered unpolarized light is the greatest.

The relation between the circular polarizance of vegetation and the angle of incidence and leaf optical properties has not been elucidated. In the past, various studies have investigated the circular polarization scattering on a molecular scale, indeed the circular polarizance is not only influenced by differential absorption but also by differential scattering. Circular Intensity Differential Scattering (CIDS) confirmed the existence of chirally organized macrostructures which show extraordinary large polarizance if the helical pitch and diameter commensurate with the wavelength [35–38]. Also in leaves, this effect was thought to play an important role on small scale circular polarizance, i.e. leading to different polarization signals for normal leaf tissue and veins [19]. As of yet, however, no systematic experimental study on the effect of incident angles on vegetation circular polarizance has been carried out. While some studies demonstrate the possibilities to detect the circular polarizance in the laboratory or in the field, these studies have either used an integrating sphere or did not record the angles of incidence and reflection (e.g. [1–3]).

In the current study we present, to the best of our knowledge, for the first time the systematic evaluation of the relation between the angle of incidence and

the full-Stokes polarizance of leaves. A better understanding of this phenomenon will be crucial in the further development of possible future remote sensing applications using circular polarizance and will ultimately aid in interpreting spectropolarimetric signals in future life-detection missions.

2 Materials and methods

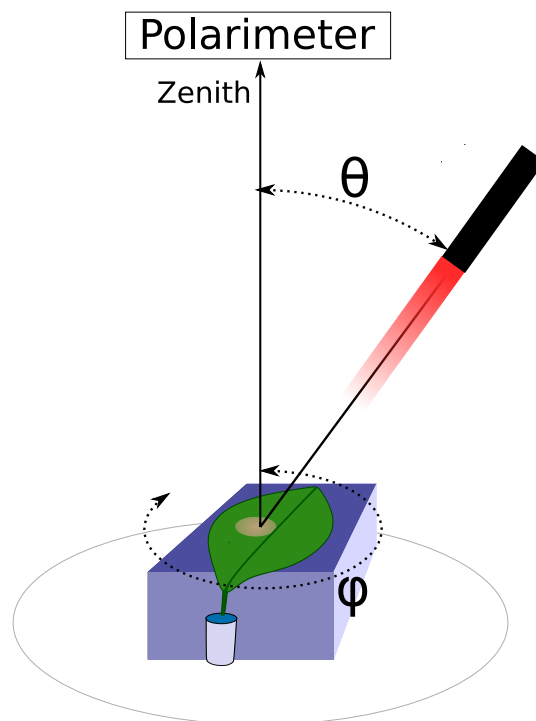


Figure 1. Schematic of the measurement setup. The detector always detects at nadir direction. θ represents the phase angle, φ represents the azimuthal angle.

The polarimeter (Hinds Instruments II/FS42-47, USA) is based on dual photoelastic modulator (PEM) modulation and is able to record the full normalized Stokes vector with minimal risk of systematic crosstalk. It consists of 2 PEMs oriented at 45° modulated at 42 and 47 kHz resonance frequencies, a prism analyzer that is 22.5° to the PEMs and a photomultiplier tube (Hamamatsu

R955, Japan).

Polarization in general is described in terms of the Stokes vector $\mathbf{S} = (I, Q, U, V)$, where I is the absolute intensity, Q and U are the unnormalized linear polarization parameters and V is the unnormalized circular polarization parameter. We describe the complete polarization states in terms of the normalized Stokes parameters Q/I , U/I and V/I , where Q/I denotes the difference between linear polarization normal and parallel to the plane of scattering, U/I denotes the difference but with a 45° offset and V/I denotes the difference between right-handed and left-handed circularly polarized light. A value of 1 or -1 indicates 100% polarized light.

Light from a 100 watt halogen light source was fed to a monochromator (Oriol instruments MS257, USA), with a FWHM of 10 nm, which is consequently fiber launched and collimated and depolarized in a head mounted on a rotating arm. The polarimeter was always detecting at nadir direction. The angle of the incident light, which is similar to the phase angle θ , varied between $10\text{-}75^\circ$ with an increment of $2.5\text{-}7.5^\circ$ varying per sample. The measured area was approximately 2 cm in diameter.

The leaves measured in this study were all picked from vegetation growing in and around the city of Bern, Switzerland, or are taken from a private indoor collection (see also Table 1 for a list of the species). The vegetation species used in this study do not represent any biome. The leaves were rinsed and padded dry prior to each measurement. The leaves were flattened and attached to a rotation stage which can change the azimuth angle φ by $0 - 360^\circ$ and was generally sampled in steps of 45° . All leaves were measured with the apex at $\varphi = 0^\circ$ and where applicable the leaf surface left of the midrib was measured. The petioles were placed in a small tube containing water in order to prevent desiccation during the measurements, which had a duration of 24-72 hours per

leaf depending on the measurement parameters.

Table 1. The measured vegetation species.

Vegetation species		
<i>Acer platanoides</i>	<i>Ficus maclellandii</i>	<i>Prunus lusitanica</i>
<i>Allium ursinum</i>	<i>Hedera helix</i>	<i>Quercus robur</i>
<i>Buddleja davidii</i>	<i>Hosta</i> sp.	<i>Reynoutria japonica</i>
<i>Calathea makoyana</i>	<i>Hosta crispula</i>	<i>Rosa</i> sp.
<i>Capsicum chinense</i>	<i>Hosta plantaginea</i>	<i>Rumex obtusifolius</i>
<i>Castanea sativa</i>	<i>Lonicera maackii</i>	<i>Schefflera actinophylla</i>
<i>Cornus alba</i>	<i>Mandevilla sanderi</i>	<i>Scindapsus pictus</i>
<i>Dypsis lutescens</i>	<i>Prunus avium</i>	<i>Syringa vulgaris</i>
<i>Epimedium alpinum</i>	<i>Prunus laurocerasus</i>	<i>Viola odorata</i>

As Stokes I was not recorded quantitatively in this study, we present a typical vegetation reflectance spectrum in Figure 2, to allow for comparison between the location of the pigment absorption bands and the presented polarizance data.

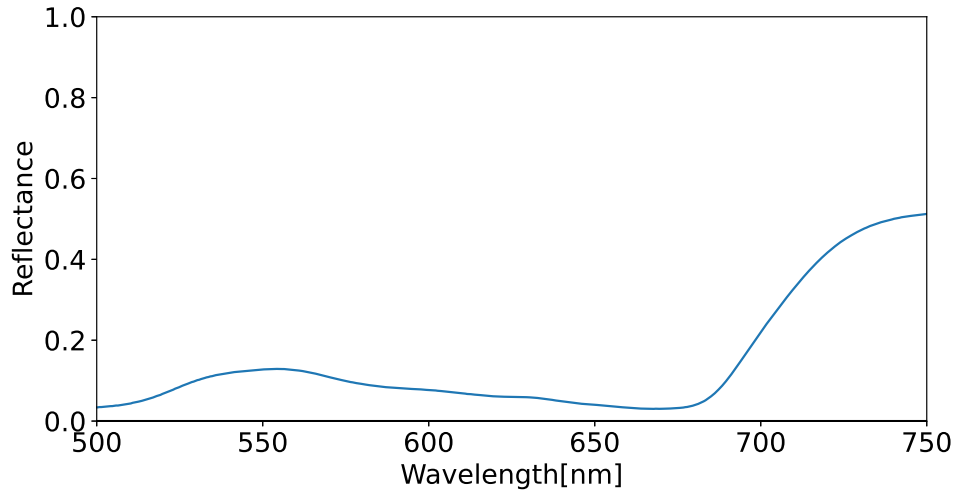


Figure 2. Typical vegetation reflectance spectrum for comparison.

3 Results

3.1 Species

Multiple different species were measured (see also Table 1) in this study. We show some representative full-Stokes polarization spectra of some of these species in Figure 3 and present the average of 27 species as the vegetation polarization biosignature in the rest of this study. The averaged full-Stokes polarization spectra of all the leaves is shown in Figure 4, while the polarization spectra of all individual leaves is shown in the appendix. Differences between the species can be observed, most notable in terms of polarization magnitude. For instance, *Rosa* sp. has both a very low Q/I and V/I even at high phase angles, with a maximum Q/I of 0.30 at a phase angle of 75° and V/I of $9.1 * 10^{-4}$ at a phase angle of 60° . On the other hand, *Viola odorata* has a much higher linear and circular polarizance, with a Q/I of 0.53 at a phase angle of 75° and a V/I of $5.9 * 10^{-3}$ at a phase angle of 45° .

For some species such as *Acer platanoides* and *Viola odorata* the positive psi-type circular polarization band remained virtually unchanged with changes in measurement geometry, whereas this effect was much larger for instance for *Rosa* sp. and *Calathea makoyana*. Contrarily, the phase angle dependency of the negative psi-type band was very small for *Calathea makoyana* but much larger for *Acer platanoides*. Important here is the difference between these two bands, which we describe as the polarization edge below.

3.2 Effects of the phase angle

We show in Figure 4 (**A**,**B** and **C**) the average linear and circular polarization spectra (Q/I , U/I and V/I respectively) of 27 different leaves per phase angle. Figure 4 (**C**,**D** and **E**) represents the same data visualized in a 2-D display.

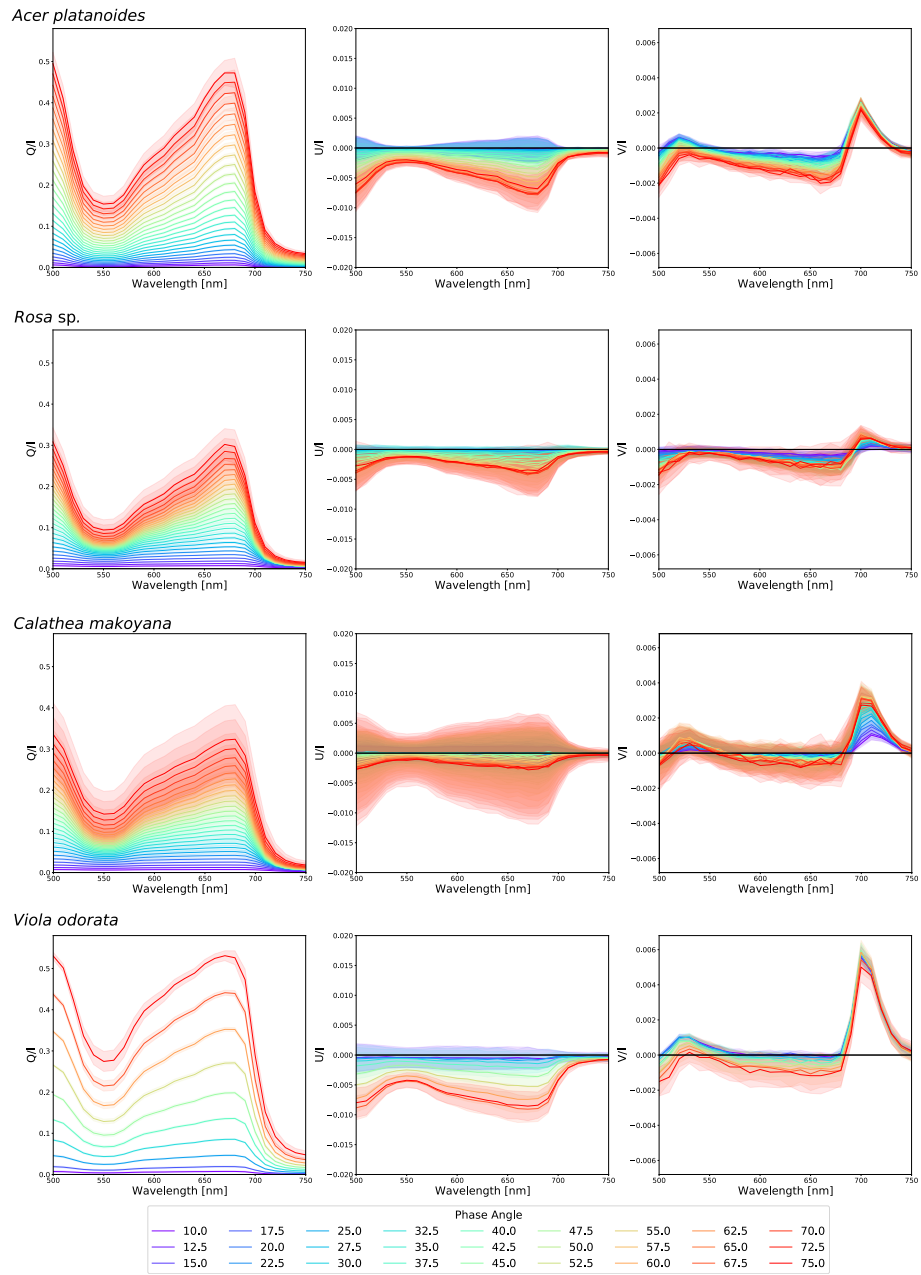


Figure 3. The polarization spectra Q/I , U/I and V/I of *Acer platanoides*, *Rosa* sp., *Calathea makoyana* and *Viola odorata* averaged over azimuth. The colors represent the different phase angles and the shaded areas denote the standard deviation.

Selected wavelengths versus the phase angle are shown in Figure 5 for Q/I (A), U/I (B) and V/I (C). The wavelengths that were selected are the maximum and minimum magnitude of the linear polarizance (670 nm and 750 nm) and the maximum magnitudes of the positive psi-type band in the blue (530 nm) and the positive and negative psi-type bands in the red (670 nm and 700 nm respectively).

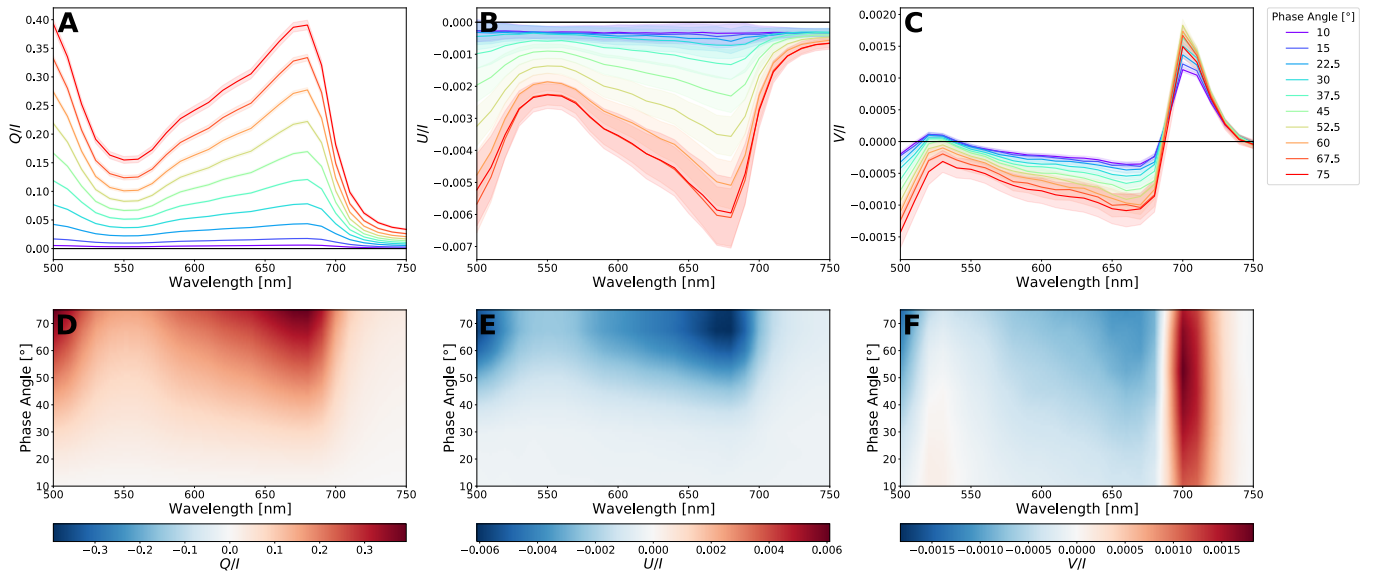


Figure 4. The average polarization spectra Q/I (A,& D) U/I (B & E) and V/I (C & F) of 27 leaves of different species averaged over azimuth. In the upper panels, the colors represent the different phase angles and the shaded areas denote the standard error.

For all wavelengths, Q/I gradually increases with increasing increment angles (see also Figure 4 (A and D) and Figure 5 (A)). The spectral features of Q/I closely resembles the inverse scalar reflectance spectrum, with low polarizance in the green (550 nm) and in the near-infrared (> 700 nm). Additionally, the linear polarizance was especially large around the chlorophyll absorption band. This general inverse relation between the linear polarization and the albedo is consistent with the Umov effect [39] and results from the attenuation of multiple

scattered light in the leaf's interior (see also Figure 2 for the general vegetation reflectance). For 670 nm, the wavelength where the linear polarizance has the largest amplitude, the polarizance increased from on average $6 * 10^{-3}$ (or 0.6%) at a 10° inclination angle to a polarizance of 0.39 (or 39%) at a phase angle of 75° . For 750 nm, this increased from $9 * 10^{-4}$ (0.09%) to 0.03 (3%).

The normalized Stokes parameter U/I shows a different spectral dependency on the phase angle (Figure 4 (B and E) and Figure 5 (B)). Essentially, the U/I appears similar to Q/I at larger phase angles. At 670 nm, where U/I has the largest magnitude, the polarizance is $3 * 10^{-4}$. Unlike Q/I , however, U/I stays relatively small ($7 * 10^{-4}$) and free of any spectral features until a phase angle of 30° . Between 30° and 67.5° the polarizance gradually increases, reaching a maximum value of $5.9 * 10^{-3}$ after which it flattens out.

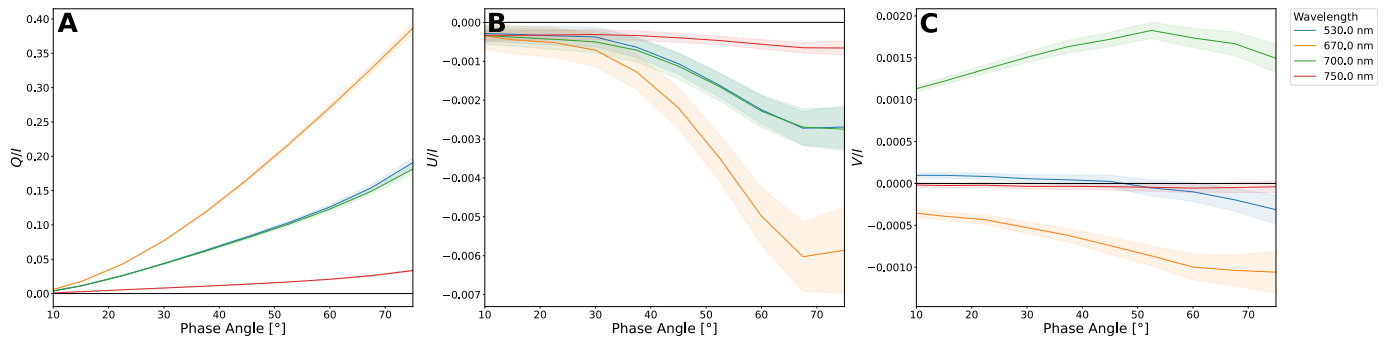


Figure 5. The polarizance, Q/I (A), U/I (B) and V/I (C), versus phase angle for selected wavelengths. Shaded areas denote the standard error.

The circular polarizance V/I is in comparison with the linear polarizance (Q/I and U/I) much less sensitive to changes in the phase angle, as can be seen in Figure 4 (C and F) and Figure 5 (C). A small positive band can be observed around ~ 510 - 540 nm (Figure 4 (C and F)), which is the psi-type band in blue stemming from the macro-organization of the pigment system. Two more psi-type bands can be observed: a negative band with the largest magnitude around 670 nm and a positive band with a peak magnitude around 700 nm.

Interestingly, while the positive band has its highest magnitude around 52.5° , with an amplitude of $1.9 * 10^{-3}$ a similar response is not observed for the negative band. The amplitude of the negative band flattens out after 60° with a maximum amplitude of $-1.1 * 10^{-3}$. Typically the blue psi-type circular polarizance band is much smaller than the psi-type bands at longer wavelengths, as can also be seen in our data. While the band keeps a similar spectral shape, the whole band increasingly becomes more negative with increasing phase angles.

3.3 Effects of the azimuthal rotations

All leaves were measured over a full 360° rotation in steps of 45° . In Figure 6 we show the non-azimuthal averaged measurements per wavelength and phase angle for Stokes Q/I . Figures 7 and 8 show these results for U/I and V/I respectively. The 26 polar plots present the different wavelengths that were measured. For each plot, the radius r represents the phase angle, while the azimuthal rotation is provided by φ .

For Q/I the variation in polarizance per azimuthal rotation is minimal although slightly increased with increasing phase angles. The difference in polarizance was the highest around the chlorophyll absorbance band (670 nm). For a phase angle of 75° , the polarizance at an azimuth of 0° and 180° was 0.43, while this was 0.37 for an azimuth of 45° and 225° . At smaller phase angles no significant differences were observed.

For U/I the differences in polarizance per azimuthal rotation were larger compared to Q/I as is shown in Figure 7. On average, the polarizance was the highest at an azimuth of 135° and 315° , while smallest at an azimuth of 45° and 225° . For example, at a phase angle of 75° , U/I was -0.012 at 315° and only $-1.9 * 10^{-3}$ at 45° . At an azimuth of 45° and 225° , Stokes U/I was positive at lower phase angles ($10 - 37.5^\circ$). For low phase angles ($10 - 30^\circ$) this results in

an azimuthal average with no significant polarization signals (see also Figure 4). For many individual species, also at higher phase angles both positive and negative U/I was observed depending on the azimuthal rotation. This results in a per species U/I signal, averaged over azimuth, that also at high phase angles is not always significant (see also the appendix for the rotational averages of the individual species).

Stokes V/I (see also Figure 8) shows small variations in polarizance per

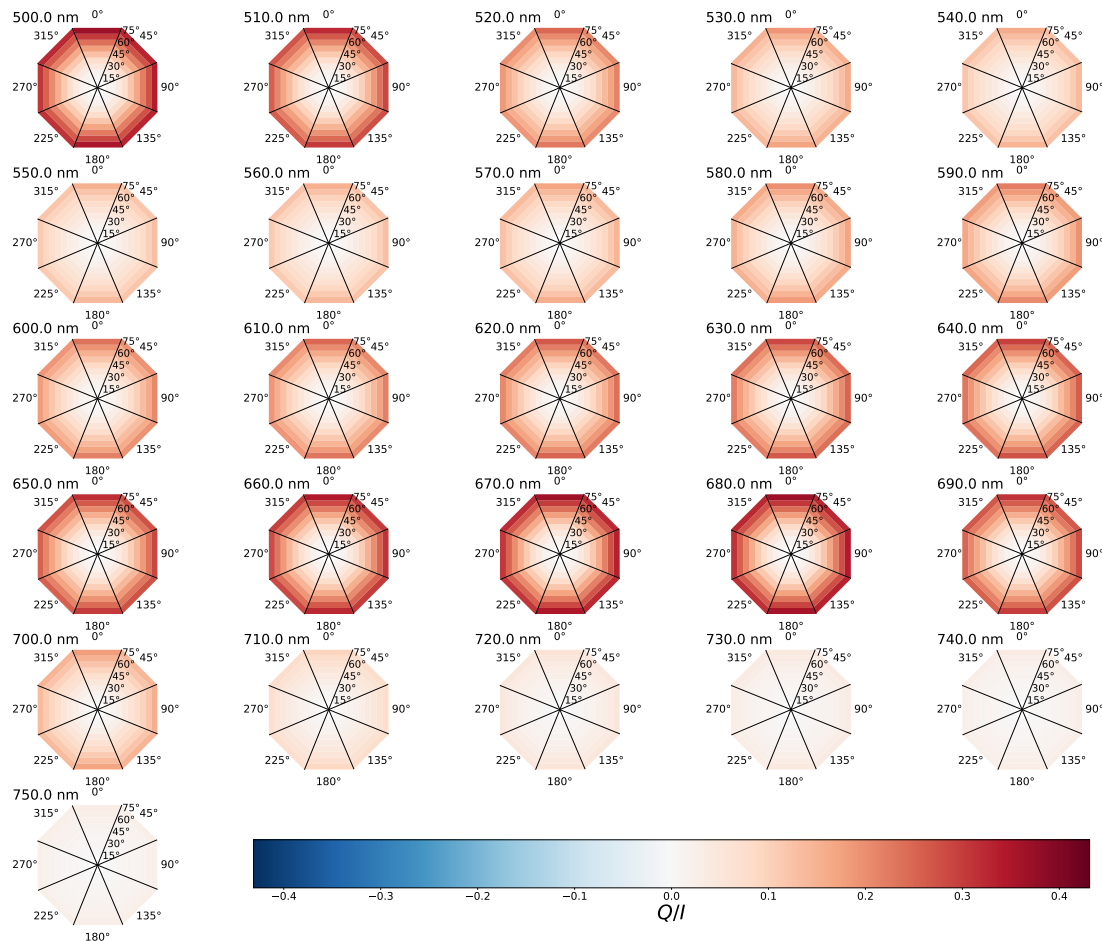


Figure 6. Polar plots per wavelength of the normalized Stokes parameter Q/I for the average of 27 leaves. The phase angle is given by the radial coordinate and the azimuth by the angular coordinate.

azimuthal rotation. While at lower phase angles there are no significant variations, at phase angles above 45° the polarizance was more slightly more negative at an azimuth of 0° and 180° and at an azimuth of 135° and 315° . On the other hand, the polarizance was more slightly more positive at an azimuth of 45° and 225° and at an azimuth of 90° and 270° . For V/I these variations seem primarily related to shifts in the zero line. When the difference between the positive and negative psi-type band per azimuth is taken no significant variations between

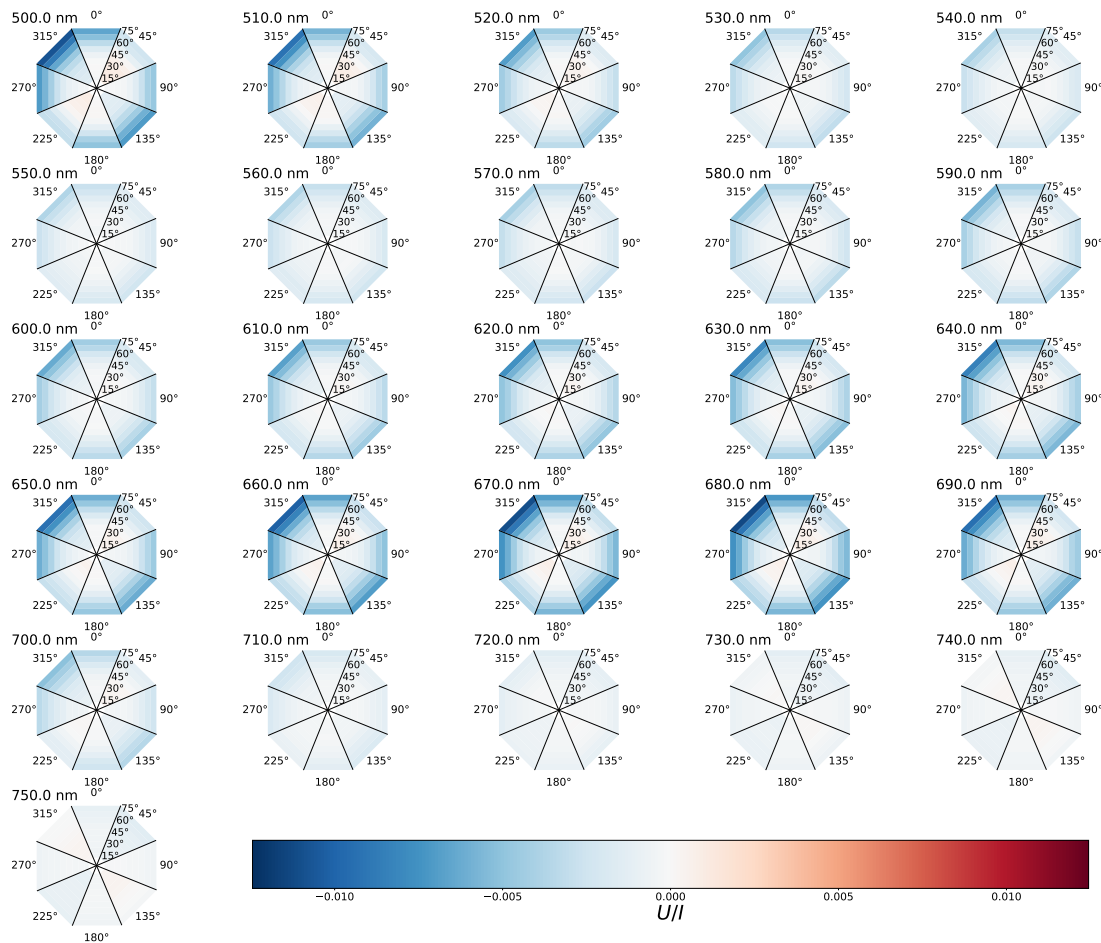


Figure 7. Polar plots of the normalized Stokes parameter U/I per wavelength for the average of 27 leaves. The phase angle is given by the radial coordinate and the azimuth by the angular coordinate.

the azimuthal rotations are observed.

In Figure 9 we show the values for Stokes Q/I (**A** and **D**), U/I (**B** and **E**) and V/I (**C** and **F**) per azimuth versus the average over all rotations. In the upper panels (**A**, **B** and **C**) the color of the data points represent the azimuth angles, while in the lower panels (**D**, **E** and **F**) the same data is shown with the colors representing the phase angles.

It is clearly visible that some azimuthal directions have a higher or lower

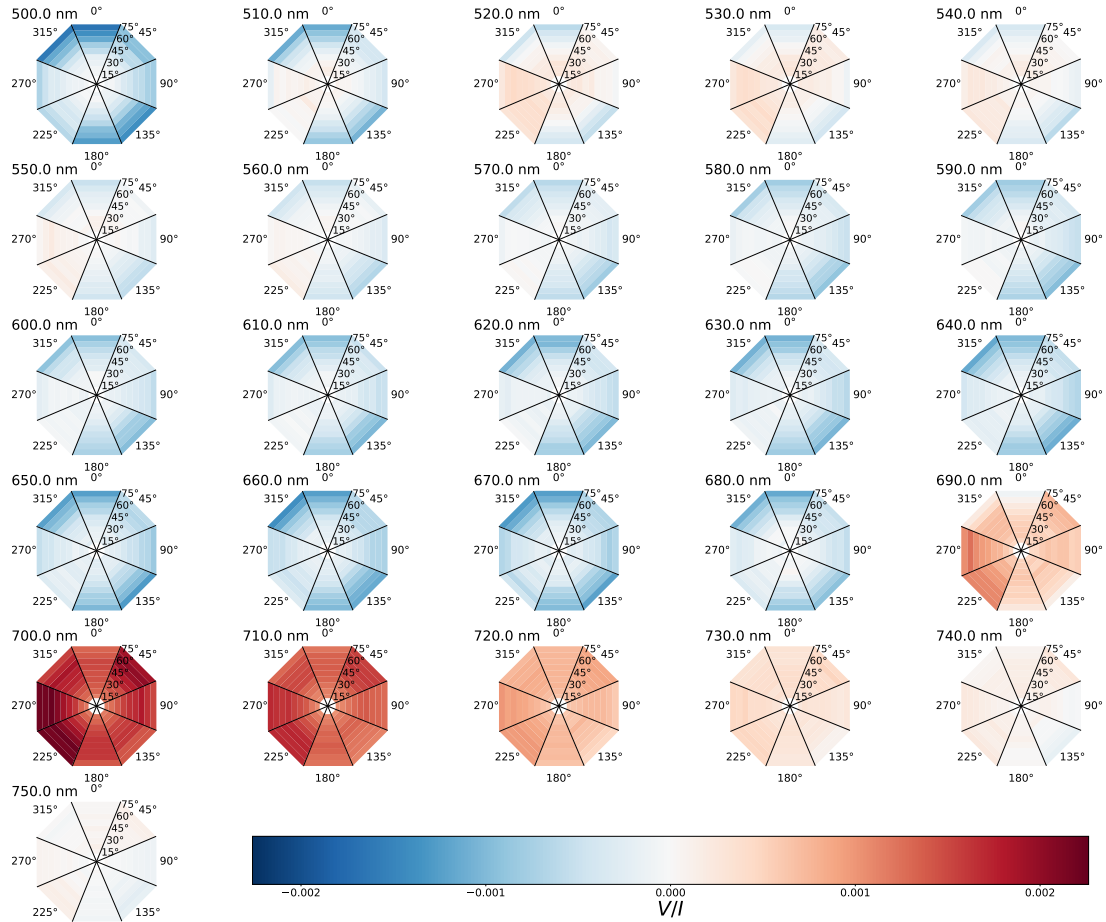


Figure 8. Polar plots of the normalized Stokes parameter V/I per wavelength for the average of 27 leaves. The phase angle is given by the radial coordinate and the azimuth by the angular coordinate.

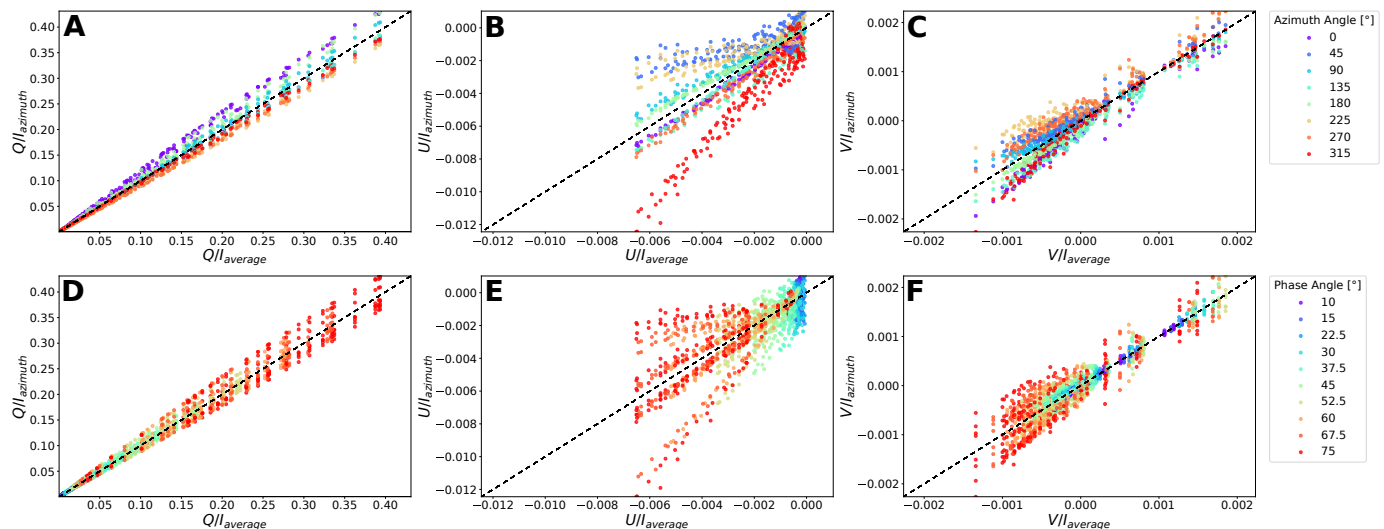


Figure 9. The normalized Stokes parameters Q/I (**A** and **D**), U/I (**B** and **E**) and V/I (**C** and **F**) per leaf azimuthal measurement vs the leaf average over all azimuthal angles. In panels **A**, **B** and **C** the colors indicate the azimuth angle. Panels **D**, **E** and **F** show the same data but the colors indicate the different phase angles.

polarizance than the rotational average. An extreme for a direction in one of the Stokes parameters does not lead to a similarly high or low value in the other parameters. The differences between the azimuthal directions and the average increase with increasing phase angles (Figure 9 **D**, **E** and **F**) as is also shown in Figure 4.

3.4 Polarization Edge

Similar to the vegetation red-edge, which is the steep increase in scalar reflectance between the chlorophyll absorption band in the red (around approximately 670 nm, see Figure 2) and the region of maximum reflectance in the near-infrared (reached after approximately 750 nm, see Figure 2), the strength of the polarization signals can be described by their 'polarization edge'. We have grouped Q/I and U/I together in the degrees of linear polarization ($DoLP$)

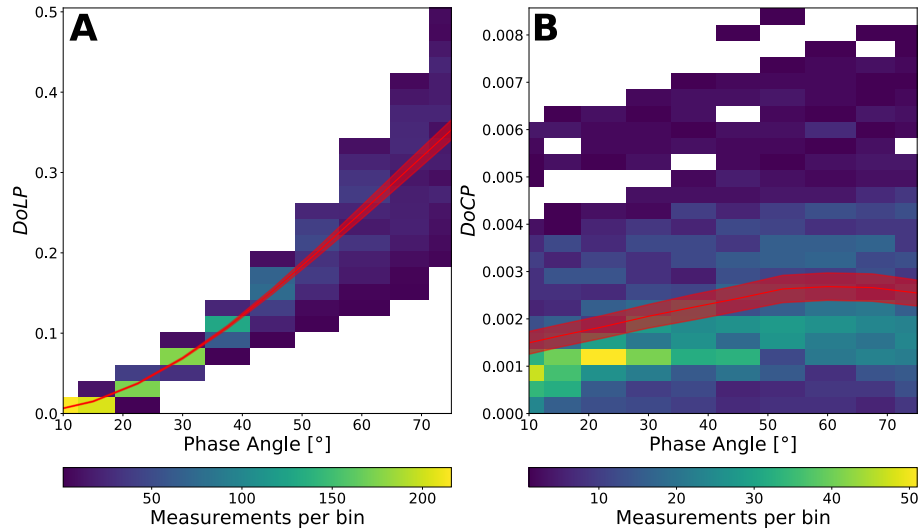


Figure 10. A 2D histogram showing the polarization edge of the linear polarization (*DoLP*) (**A**) and the circular polarization (*DoCP*) (**B**) versus the phase angle for all measurements. The red line represents the average of 27 different leaves and the red shaded area represents the standard error.

(i.e. $DoLP = \sqrt{Q^2 + U^2}/I$) which makes more sense from a biosignature point of view. For the *DoLP* we have measured the polarization edge by taking the value at 670 nm, where the polarizance is maximal for both Q/I and U/I , and subtracting it with the background polarization at 750 nm. For the circular polarization, we compute the polarization edge as the difference between the negative (670 nm) and positive (700 nm) psi-type circular polarizance band, where the absolute value is expressed as the degrees of circular polarization (*DoCP*). Note that we did not correct for the background polarization at 750 nm as due to the split signal this will only lead to a total offset in V/I but not a change in magnitude. Additionally, the magnitude at 750 nm was less than $5 * 10^{-5}$ (see also Figure 5 (C)). We show the polarization edges in Figure 10 of the linear polarization **A** and of the circular polarization **B** shown in degrees of circular polarization. The red line represents the average of 27 leaves while the edges per measurement are grouped into bins, with the amount per bin

represented by the colorbar.

For the *DoLP* the largest difference between the minimum and maximum polarizance was observed at 75° , where the edge had a magnitude of 0.35. As the maximum polarizance was still increasing with increasing phase angles it is likely that the peak polarizance and edge magnitude occurs at even higher phase angles. For the *DoCP*, the maximum edge was measured at 60° , with an average value of $2.7 * 10^{-3}$. We show the maximum and the minimum extend of the polarization edges per species in Figure 11.

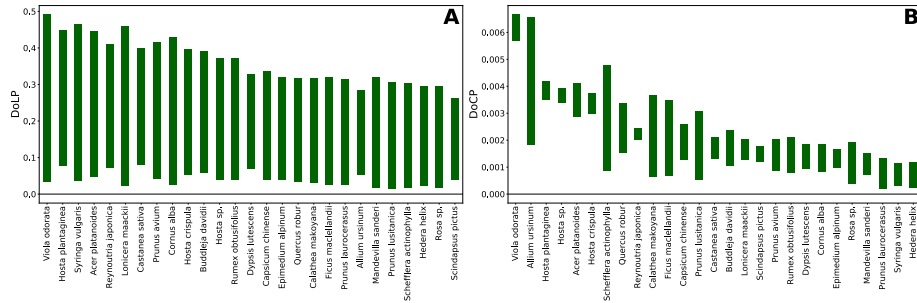


Figure 11. The maximum and minimum polarization edge over phase angle of the linear polarization (*DoLP*) (**A**) and the circular polarization (*DoCP*) (**B**) for all measured species averaged over azimuth. Data are sorted on the average edge value.

3.5 Non-vegetation polarizance

For comparison with the vegetation polarization data, we show in Figure 12 the linear (**A** and **B**) and the circular polarization spectra (**C**) versus the phase angle of 3 sand samples. Again, Figure 12 (**C,D** and **E**) represents the same data visualized in a 2-D display. Selected wavelengths, similar to those in Figure 5, versus the phase angle are shown in **G**, **H** and **I** for Q/I , U/I and V/I respectively.

Similar to vegetation, Q/I strongly increases with increasing phase angles. Also for sand, the linear polarizance correlates to its reflectance spectrum which

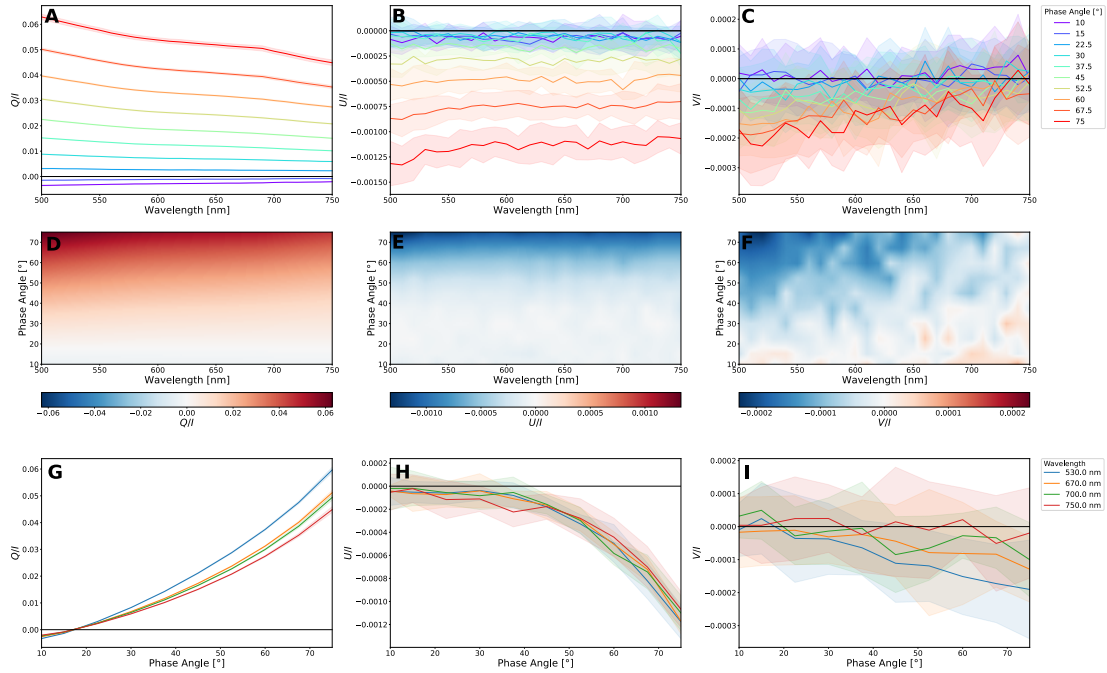


Figure 12. The average polarization spectra Q/I (A, & D) U/I (B & E) and V/I (C & F) of 3 samples of sand averaged over azimuth. In the upper panels, the colors represent the different phase angles and the shaded areas denote the standard error. In the bottom panels, the colors represent different wavelengths and the shaded areas denote the standard error.

in the visible gradually increases with increasing wavelength. At small phase angles (see also Figure 12 (G)), Q/I was negative, thus the polarization was oriented parallel to the plane of scattering. Q/I changed sign at $\sim 17^\circ$ for all measured wavelengths. We observed a similar negative Q/I at small phase angles (typically below 22.5°) for some leaves, but on average Q/I was positive for all measured wavelengths (see Figure 4 (A)).

Stokes U/I is approximately 0 for all wavelengths below a phase angle of 37.5° but then increases in overall with increasing phase angles and is spectrally featureless. The circular polarizance, too, is not showing any spectral features. Especially towards the blue V/I increases slightly with increasing phase angles, with a maximum of $-2.2 * 10^{-4}$.

4 Discussion and conclusions

We present in this study the systematic investigation of full-Stokes spectropolarimetry on leaves and its dependency on the phase angle. Importantly, while some studies and models exist for the linear polarizance of vegetation, studies showing the relationship between vegetation circular polarizance and phase angle are lacking. It has been demonstrated that circular polarimetry is able to provide an unambiguous means to detect homochiral matter, considered an important universal agnostic biosignature [3, 5]. The results in this study demonstrate that the characteristic spectropolarimetric properties of vegetation remain relatively unchanged with changes in measurement geometry, underlining the potential of circular spectropolarimetry as a means of detecting life beyond Earth.

Accounting only for the molecular phenomena, the vegetation circular polarizance should in principle be insensitive to phase angle variations. While the phase angle is important at the molecular scale and in oriented isolated constituents, which can result in very different spectral shapes [40, 41], it can be expected that these variations even out at larger scales where the chloroplasts are more randomly distributed. Leaves, however, are geometrically complex structures with many different cellular interfaces and covered by an extracellular lipid structure with varying chemical compositions that can all potentially affect its spectropolarimetric response [26, 33].

We demonstrate in the present study that the circular polarizance of vegetation is relatively insensitive to alterations in the phase angle. These results confirm previous circular spectropolarimetric field observations of vegetation canopy under overcast and cloudless sky conditions, showing a circular polarization spectrum that was virtually identical [1]. Still, the magnitude of the signal varied with changes in phase angle, where the largest differences between the negative and positive band were observed at a phase angle of 60° and the smallest

at a phase angle of 10° (Figure 10). The spectral shape of the typical split psi-type polarization, however, remained preserved. As such, integrating over a planetary disc should not yield spectral changes due to possible phase angle dependency. Additionally, it has been suggested that the vegetation circular polarizance could be a powerful tool in assessing vegetation physiology remotely [2, 18]. Remote sensing using circular spectropolarimetry will be able to directly probe the macromolecular structure of the photosynthetic apparatus and thus its functioning [18, 24] and as such could provide a powerful complementary tool in assessing effects of climate change and the monitoring of vegetation physiological state in vulnerable regions [2].

It should be noted that in some cases significant spectropolarimetric differences between species can be observed. For instance, in a *Hosta* cultivar (see Appendix) we observed a negative psi-type polarization band with a magnitude of well over $-5 * 10^{-3}$ but with a positive band of only $1 * 10^{-3}$. On the other hand we measured for a *Viola* cultivar (see Figure 3) a positive band with a magnitude of $6 * 10^{-3}$ but with a corresponding negative band less than $-1 * 10^{-4}$. Importantly, the two psi-type bands have a different physical origin, where the negative band is preferentially associated with the stacking of the thylakoid membranes inside the chloroplasts, and where the positive band is mainly associated with the lateral organization of the chiral macro-domains [23, 24]. Similar differences, where some species have much larger negative or positive bands, have been reported before, see e.g. [2, 7]. While the circular polarizance does not always provide a specific species signature and it will thus be difficult to determine the species based on the signal alone, it could potentially aid in enhancing the contrast in existing distinguishing techniques.

The linear polarizance of vegetation, too, can serve as a biosignature [31, 32]. Importantly, the linear polarization created by vegetation could be used to

enhance the contrast between the reflected light of an exoplanet and the very bright emission by its host star [32] As has been reported before (see e.g. [25, 33, 34]), vegetation linear polarization is strongly dependent on the phase angle. At a phase angle of 10° , we measured an average linear polarization of $6.4 * 10^{-3}$. At 75° the linear polarizance was much higher with a value of 0.35 which on average continued to increase. Likely the maximum average polarizance lies between 75° and two times the Brewster angle (which for leaves is 55.4° on average [42]).

In contrast to vegetation circular polarizance, the linear polarizance is more dependent on the pigments present in the leaf, rather than their molecular organization. The structural geometry of leaves can vary greatly between species and is not homogeneous. Some leaves have a thick shiny cuticle while others are abundant in trichomes (fine epidermal outgrowths or hairs). Importantly, a leaf surface is generally far from optically smooth [26]. Larger structures are shown along the veins which can undulate from the surface but many plants have surfaces with angular aspects in multiple directions. Such phenomena can affect the obtained leaf linear polarizance [25, 26]. Additionally, the interior anatomy of leaves can vary greatly between species, and can vary between leaves of the same species. While the effects of these variations on the polarization response has not been studied in depth, it is clear that they can effect the optical properties greatly and can have a large effect on scalar reflectance and transmittance [42]. It has additionally been demonstrated that linear polarization can be informative of plant physiological status [27, 28, 30].

Similar to the scalar reflectance, edges mimicking biotic matter can readily emerge in the spectropolarimetry of abiotic matter, whereas circular polarizance is less prone to such confounding factors. Consequently, while circular polarization signals of comparatively small magnitude (but can be up to a couple percent

for certain eukaryotic algae [7]), it has the potential to deliver a more robust and specific biosignature. The scalar reflectance, linear polarizance and circular polarizance are, however, very complementary tools. In the end, a confident detection of extraterrestrial life candidates will presumably have to consist of a vast range of spectroscopic techniques.

Overall, we have successfully demonstrated that the circular polarization biosignatures of vegetation are relatively insensitive to changes in phase angle, providing a promising outlook on future life detection or remote sensing applications. It will be important to compare the results in this study with controlled measurements of vegetation taken in the field. Additionally, it will be also key to incorporate the circular polarizance-phase angle relationship in (exo)planetary models with realistic surface and atmospheric components [43]. While we have only measured vegetation in this study, more primitive phototrophs also show remarkable polarization features [6]. Although it is not expected that measurements on these organisms yield different results for the circular polarization phase angle dependency, such study would be highly interesting and important in understanding the nature of especially circular polarization as a biosignature.

Acknowledgments

This work has been carried out within the framework of the National Centre of Competence in Research (NCCR), PlanetS, supported by the Swiss National Science Foundation (SNSF).

References

1. C. H. Lucas Patty, Inge Loes ten Kate, Wybren Jan Buma, Rob J. M. van Spanning, Gábor Steinbach, Freek Ariese, and Frans Snik. Circular spectropolarimetric sensing of vegetation in the field: Possibilities for the remote detection of extraterrestrial life. *Astrobiology*, 19(10):1221–1229, oct 2019.
2. C. H. Lucas Patty, Jonas G. Kühn, Petar H. Lambrev, Stefano Spadaccia, H. Jens Hoeijmakers, Christoph Keller, Willeke Mulder, Vidhya Pallichadath, Olivier Poch, Frans Snik, Daphne M. Stam, Antoine Pommerol, and Brice O. Demory. Biosignatures of the earth i. airborne spectropolarimetric detection of photosynthetic life. *Astronomy & Astrophysics*, jun 2021.
3. William B Sparks, James Hough, Thomas A Germer, Feng Chen, Shiladitya DasSarma, Priya DasSarma, Frank T Robb, Nadine Manset, Ludmilla Kolokolova, Neill Reid, et al. Detection of circular polarization in light scattered from photosynthetic microbes. *Proceedings of the National Academy of Sciences*, 106(19):7816–7821, 2009.
4. L. Rossi and D. M. Stam. Circular polarization signals of cloudy (exo)planets. *Astronomy & Astrophysics*, 616:A117, aug 2018.
5. C. H. Lucas Patty, Inge Loes ten Kate, William B. Sparks, and Frans Snik. Remote sensing of homochirality: a proxy for the detection of extraterrestrial life. In Prasad Polavarapu, editor, *Chiral Analysis, Second Edition: Advances in Spectroscopy, Chromatography and Emerging Methods*, chapter 2, pages 29–69. Elsevier Science, 2018.
6. William B. Sparks, M. Niki Parenteau, Robert E. Blankenship, Thomas A. Germer, C. H. Lucas Patty, Kimberly M. Bott, Charles M. Telesco, and

-
- Victoria S. Meadows. Spectropolarimetry of primitive phototrophs as global surface biosignatures. *Astrobiology*, 21(2):219–234, feb 2021.
7. C. H. Lucas Patty, Freek Ariese, Wybren Jan Buma, Inge Loes ten Kate, Rob J. M. van Spanning, and Frans Snik. Circular spectropolarimetric sensing of higher plant and algal chloroplast structural variations. *Photosynthesis Research*, pages 1–11, 2018.
 8. DV Grishin, DD Zhdanov, MV Pokrovskaya, and NN Sokolov. D-amino acids in nature, agriculture and biomedicine. *All Life*, 13(1):11–22, 2020.
 9. Marian Novotny and Gerard J Kleywegt. A survey of left-handed helices in protein structures. *Journal of molecular biology*, 347(2):231–241, 2005.
 10. Radu Popa. *Between necessity and probability: searching for the definition and origin of life*. Springer Science & Business Media, 2004.
 11. William A Bonner. Chirality and life. *Origins of Life and Evolution of the Biosphere*, 25(1-3):175–190, 1995.
 12. Farshid Jafarpour, Tommaso Biancalani, and Nigel Goldenfeld. Noise-induced mechanism for biological homochirality of early life self-replicators. *Physical Review Letters*, 115(15):158101, 2015.
 13. George Wald. The origin of optical activity. *Annals of the New York Academy of Sciences*, 69(2):352–368, 1957.
 14. AJ MacDermott. 8.2 perspective and concepts: Biomolecular significance of homochirality: The origin of the homochiral signature of life. pages 11–38, 2012.
 15. David Avnir. Critical review of chirality indicators of extraterrestrial life. 92:101596.

-
16. Gerald D Fasman. *Circular dichroism and the conformational analysis of biomolecules*. Springer Science & Business Media, 2013.
 17. J. C. Kemp, G. D. Henson, C. T. Steiner, and E. R. Powell. The optical polarization of the sun measured at a sensitivity of parts in ten million. *Nature*, 326(6110):270–273, 1987.
 18. C. H. Lucas Patty, Luuk J. J. Visser, Freek Ariese, Wybren Jan Buma, William B. Sparks, Rob J. M. van Spanning, Wilfred F. M. Röling, and Frans Snik. Circular spectropolarimetric sensing of chiral photosystems in decaying leaves. *Journal of Quantitative Spectroscopy and Radiative Transfer*, 189:303–311, 2017.
 19. C. H. Lucas Patty, David A. Luo, Frans Snik, Freek Ariese, Wybren Jan Buma, Inge Loes ten Kate, Rob J. M. van Spanning, William B. Sparks, Thomas A. Germer, Győző Garab, and Michael W. Kudenov. Imaging linear and circular polarization features in leaves with complete Mueller matrix polarimetry. *Biochimica et Biophysica Acta (BBA) - General Subjects*, 1862(6), 2018.
 20. David Keller and Carlos Bustamante. Theory of the interaction of light with large inhomogeneous molecular aggregates. II. psi-type circular dichroism. *The Journal of Chemical Physics*, 84(6):2972–2980, 1986.
 21. Virginijus Barzda, Laszlo Mustardy, and Gyozo Garab. Size dependency of circular dichroism in macroaggregates of photosynthetic pigment-protein complexes. *Biochemistry*, 33(35):10837–10841, 1994.
 22. Győző Garab. Linear and circular dichroism. In *Biophysical Techniques in Photosynthesis*, pages 11–40. Kluwer Academic Publishers, 1996.
 23. Győző Garab and Herbert van Amerongen. Linear dichroism and circular

-
- dichroism in photosynthesis research. *Photosynthesis Research*, 101(2-3):135–146, 2009.
24. Petar H. Lambrev and Parveen Akhtar. Macroorganisation and flexibility of thylakoid membranes. *Biochemical Journal*, 476(20):2981–3018, oct 2019.
25. Vern C Vanderbilt, Lois Grant, and CST Daughtry. Polarization of light scattered by vegetation. *Proceedings of the IEEE*, 73(6):1012–1024, 1985.
26. Lois Grant. Diffuse and specular characteristics of leaf reflectance. 22(2):309–322.
27. Vern C. Vanderbilt, Craig S. T. Daughtry, Meredith K. Kupinski, Christine L. Bradley, Andrew N. French, Kevin Bronson, Russell A. Chipman, and Robert P. Dahlgren. Estimating the relative water content of leaves in a cotton canopy. In Frans Snik and Joseph A. Shaw, editors, *Polarization Science and Remote Sensing VIII*, volume 10407, page 104070Z. International Society for Optics and Photonics, SPIE, 2017.
28. Vern Vanderbilt, Craig Daughtry, and Robert Dahlgren. Polarization to estimate leaf surface reflectance. In *Polarization Science and Remote Sensing IX*, volume 11132, page 1113205. International Society for Optics and Photonics, 2019.
29. Lois Grant, C.S.T. Daughtry, and V.C. Vanderbilt. Polarized and specular reflectance variation with leaf surface features. *Physiologia Plantarum*, 88(1):1–9, 1993.
30. Ce Yao, Shan Lu, and Zhongqiu Sun. Estimation of leaf chlorophyll content with polarization measurements: Degree of linear polarization.

Journal of Quantitative Spectroscopy and Radiative Transfer, 242:106787, feb 2020.

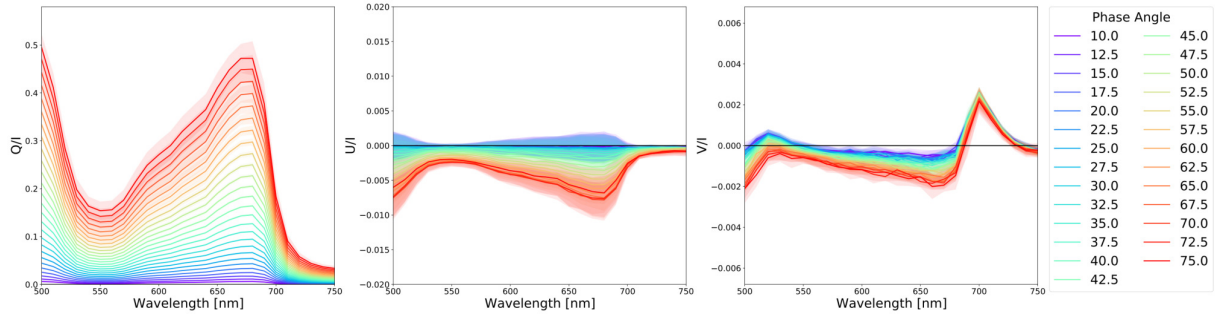
31. Svetlana V Berdyugina, Jeff R Kuhn, David M Harrington, Tina Šantl-Temkiv, and E John Messersmith. Remote sensing of life: polarimetric signatures of photosynthetic pigments as sensitive biomarkers. *International Journal of Astrobiology*, 15(01):45–56, 2016.
32. Dora Klindžić, Daphne Stam, Frans Snik, Christoph Keller, Vidhya Pallichadath, Chris van Dijk, Marco Esposito, and Dirk van Dam. Loupe: Observing the earth from the moon to prepare for detecting life on earth-like exoplanets.
33. V. C. Vanderbilt, L. Grant, and S. L. Ustin. Polarization of light by vegetation, 1991.
34. Jouni I. Peltoniemi, Maria Gritsevich, and Eetu Puttonen. *Reflectance and polarization characteristics of various vegetation types*. Springer Nature, 2015.
35. Gyozo Garab, Sam Wells, Laura Finzi, and Carlos Bustamante. Helically organized macroaggregates of pigment-protein complexes in chloroplasts: evidence from circular intensity differential scattering. *Biochemistry*, 27(16):5839–5843, 1988.
36. Gyozo Garab, Agnes Faludi-Daniel, John C. Sutherland, and Geoffrey Hind. Macroorganization of chlorophyll a/b light-harvesting complex in thylakoids and aggregates: information from circular differential scattering. *Biochemistry*, 27(7):2425–2430, 1988.
37. Carlos Bustamante, Marcos F. Maestre, and David Keller. Expressions

-
- for the interpretation of circular intensity differential scattering of chiral aggregates. *Biopolymers*, 24(8):1595–1612, aug 1985.
38. Carlos Bustamante, Ignacio Tinoco, and Marcos F Maestre. Circular differential scattering can be an important part of the circular dichroism of macromolecules. *Proceedings of the National Academy of Sciences*, 80(12):3568–3572, 1983.
39. N.A. Umov. Chromatische depolarisation durch lichtzerstreuung. *Phys. Z*, 6:674–676, 1905.
40. G Garab, L Finzi, and C Bustamante. Differential polarization imaging of chloroplasts: Microscopic and macroscopic linear and circular dichroism. *Light in Biology and Medicine*, 2, 1991.
41. Laura Finzi, Carlos Bustamante, Gyözö Garab, and Ching-Bo Juang. Direct observation of large chiral domains in chloroplast thylakoid membranes by differential polarization microscopy. *Proceedings of the National Academy of Sciences*, 86(22):8748–8752, 1989.
42. Stéphane Jacquemoud and Susan Ustin. Measurement of leaf optical properties. In *Leaf Optical Properties*, pages 74–123. Cambridge University Press.
43. A. Groot, L. Rossi, V. J. H. Trees, J. C. Y. Cheung, and D. M. Stam. Colors of an earth-like exoplanet-temporal flux and polarization signals of the earth. *Astronomy & Astrophysics*, 640:A121, aug 2020.

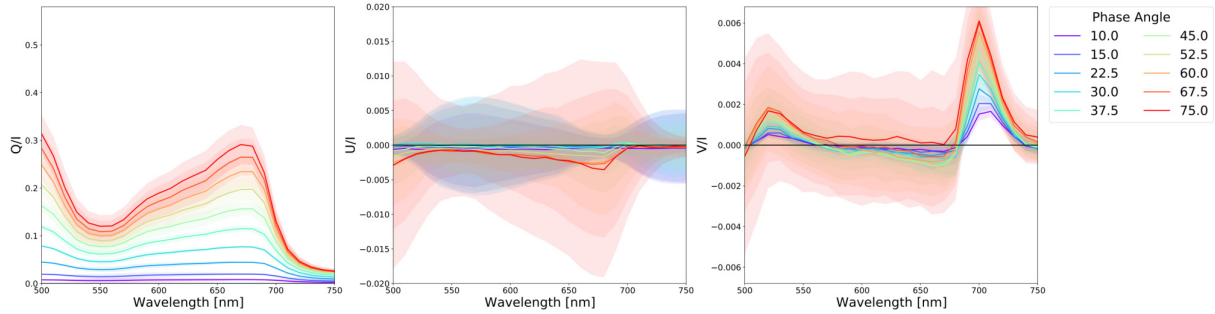
5 Supplementary Material

The polarization spectra of all leaves used in this study averaged over azimuth. The colors represent the different phase angles and the shaded areas denote the standard deviation.

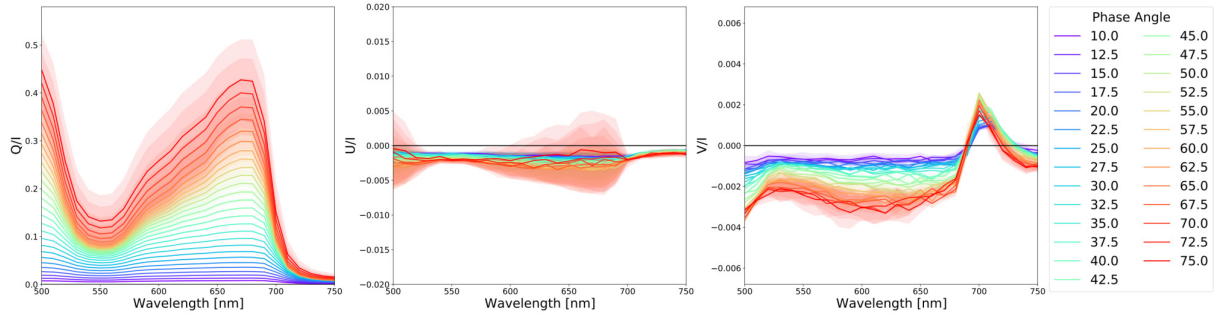
Acer platanoides



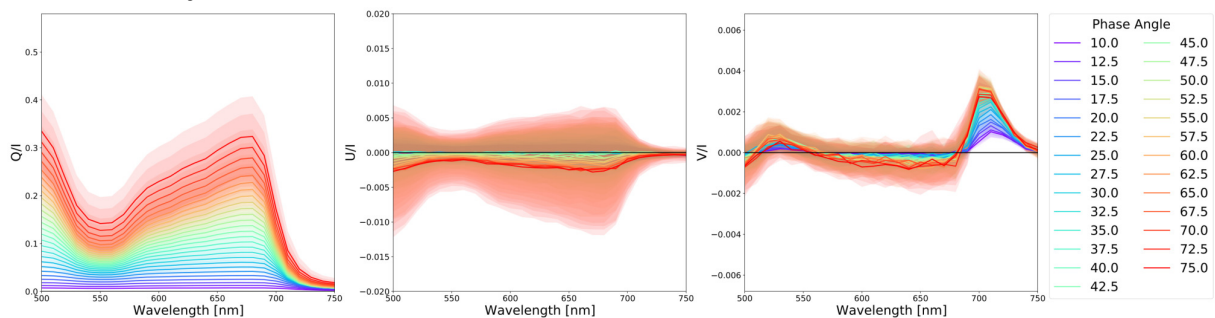
Allium ursinum



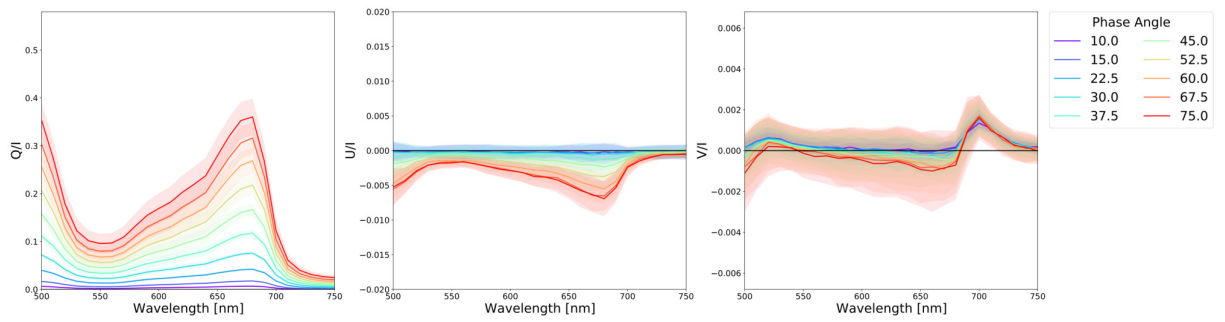
Buddleja davidii



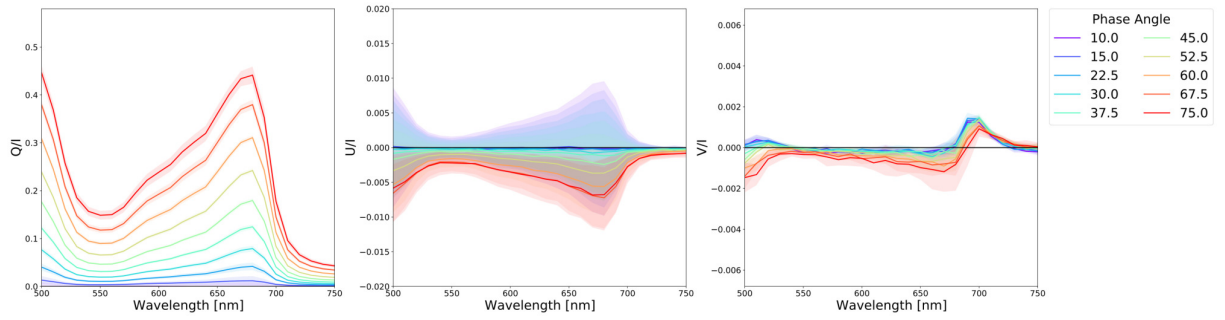
Calathea makoyana



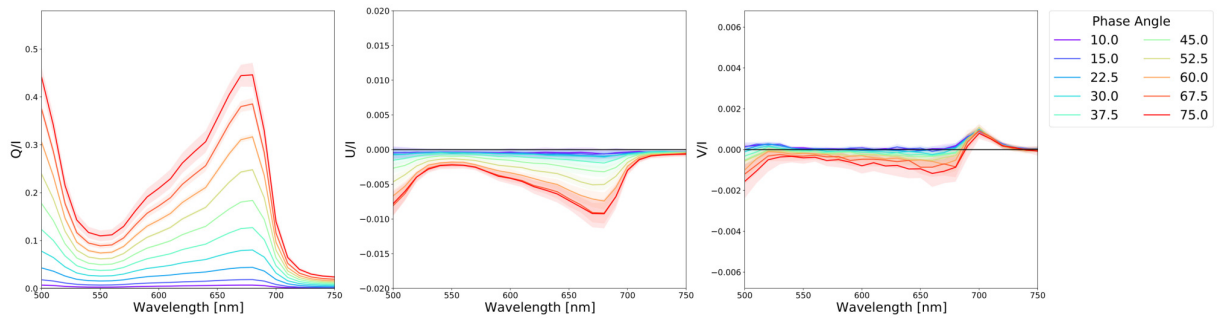
Capsicum chinense



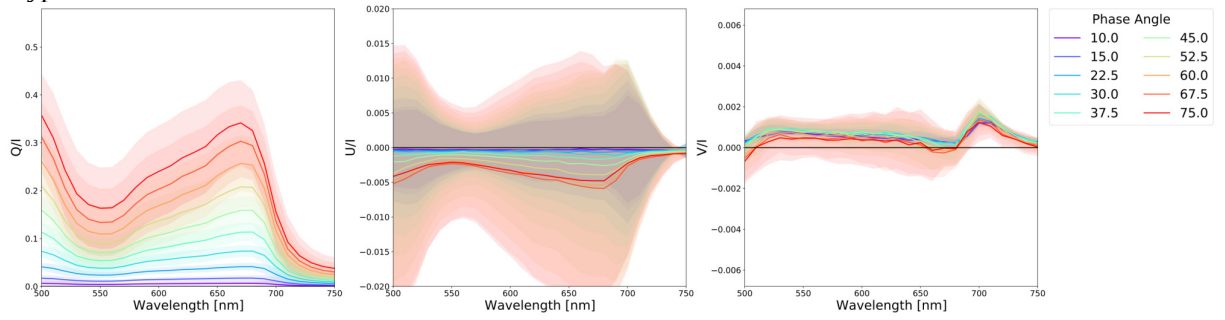
Castanea sativa



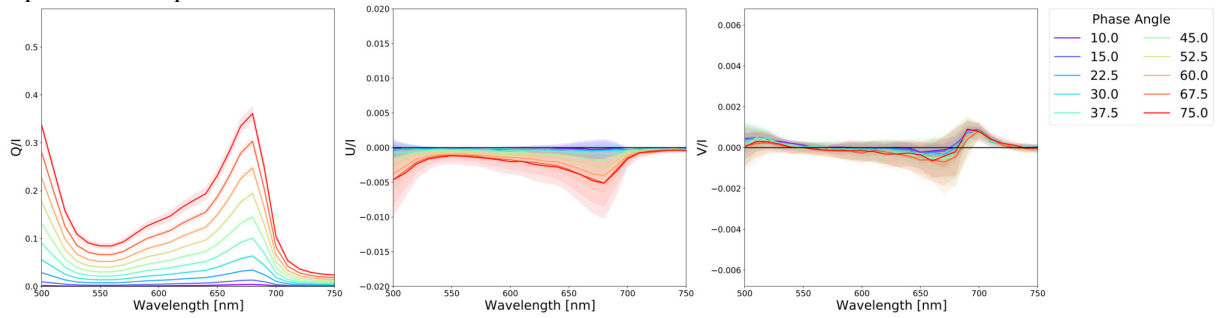
Cornus alba



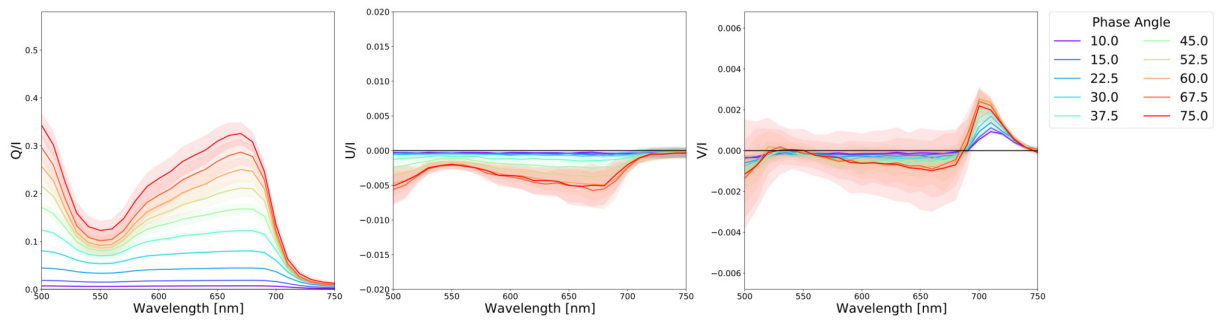
Dypsis lutescens



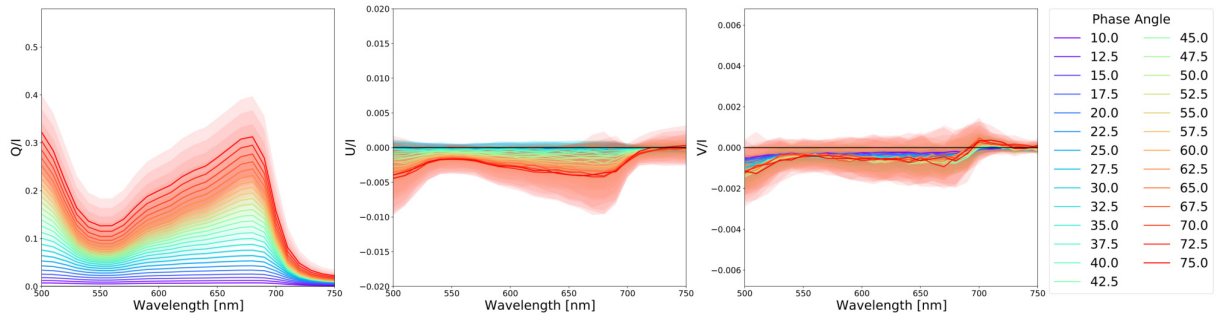
Epimedium alpinum



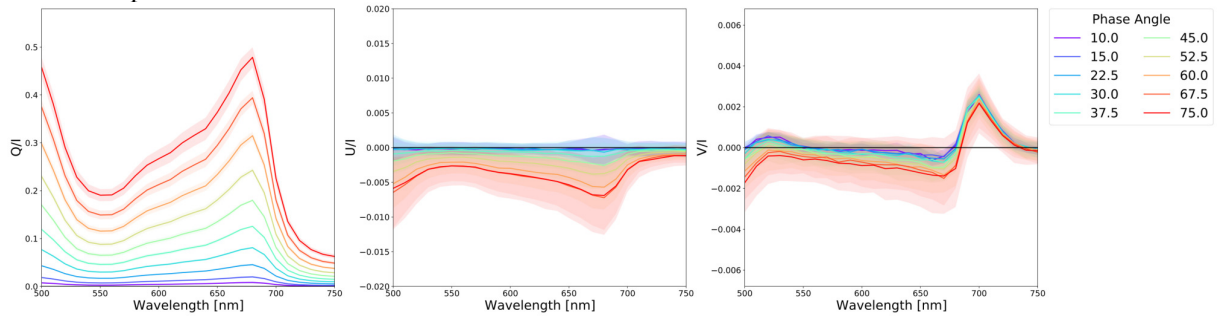
Ficus maclellandii



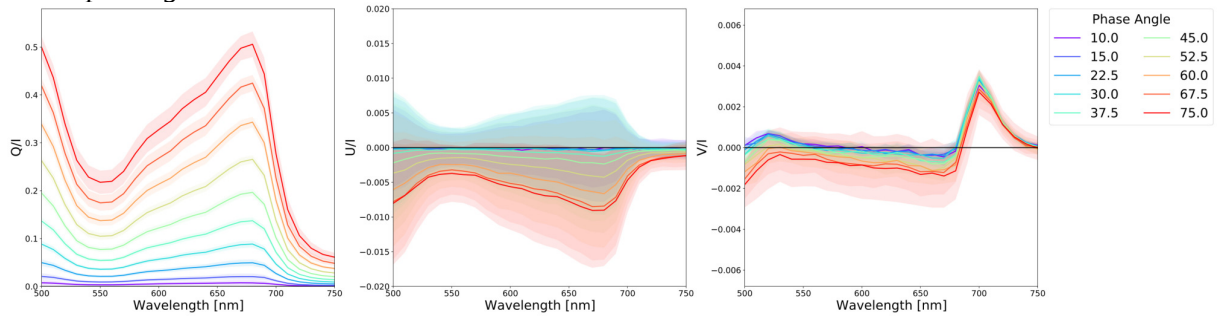
Hedera helix



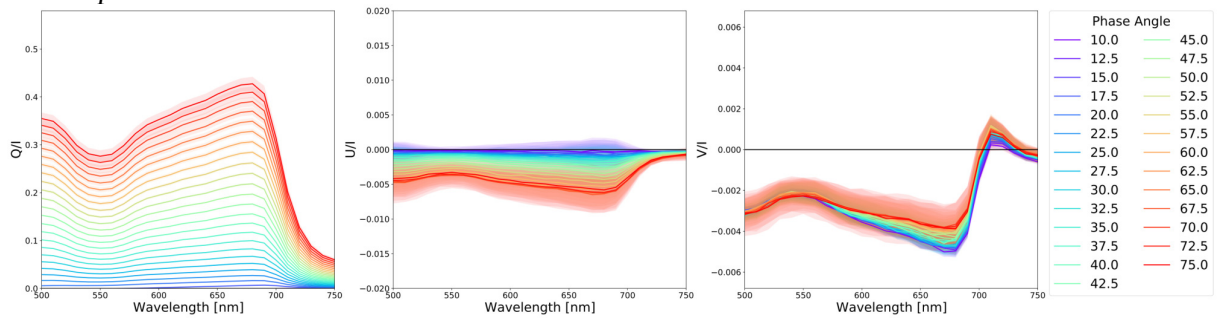
Hosta crispula



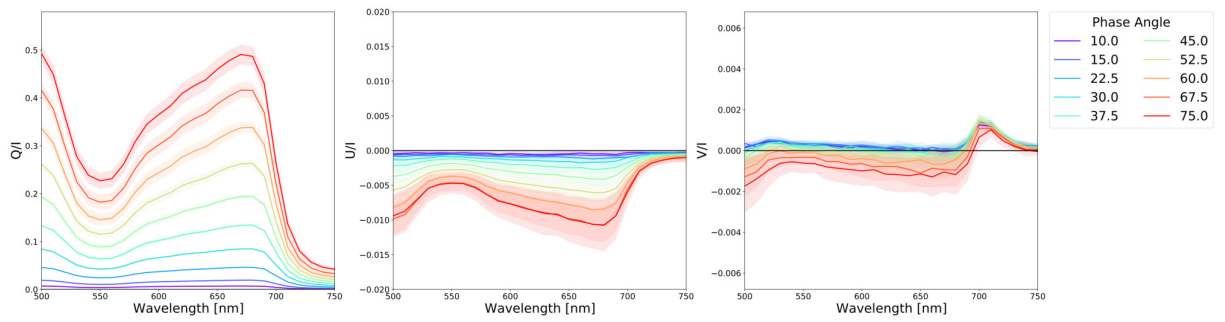
Hosta plantaginea



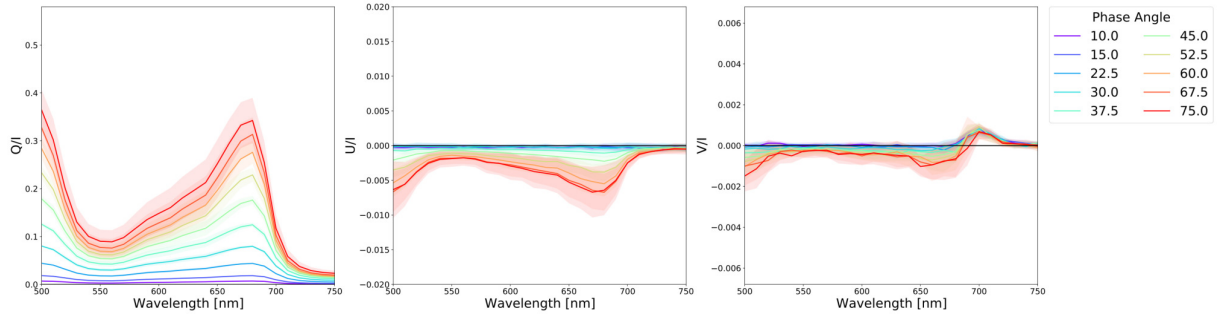
Hosta sp.



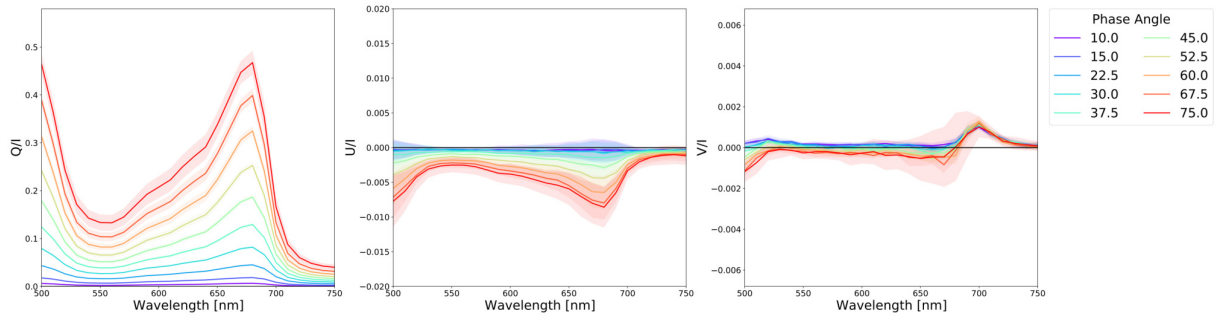
Lonicera maackii



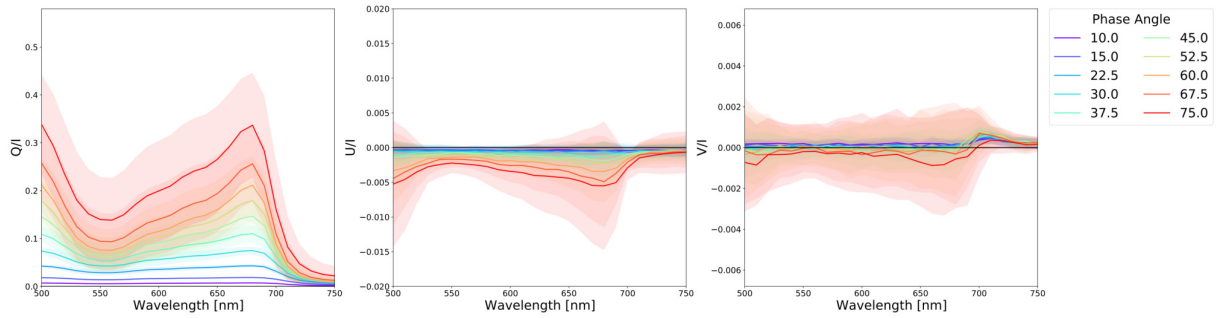
Mandevilla sanderi



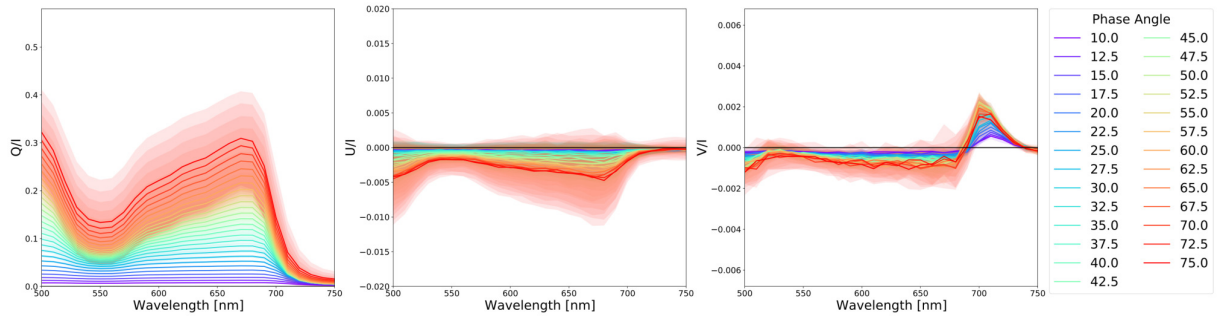
Prunus avium



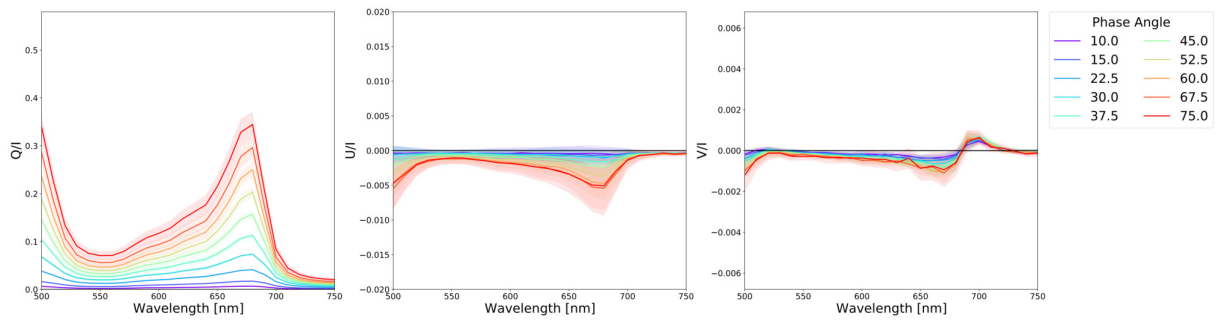
Prunus laurocerasus



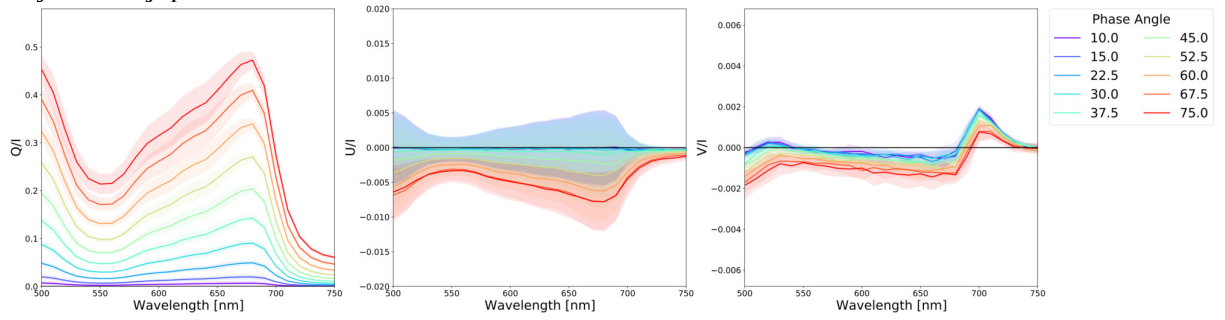
Prunus lusitanica



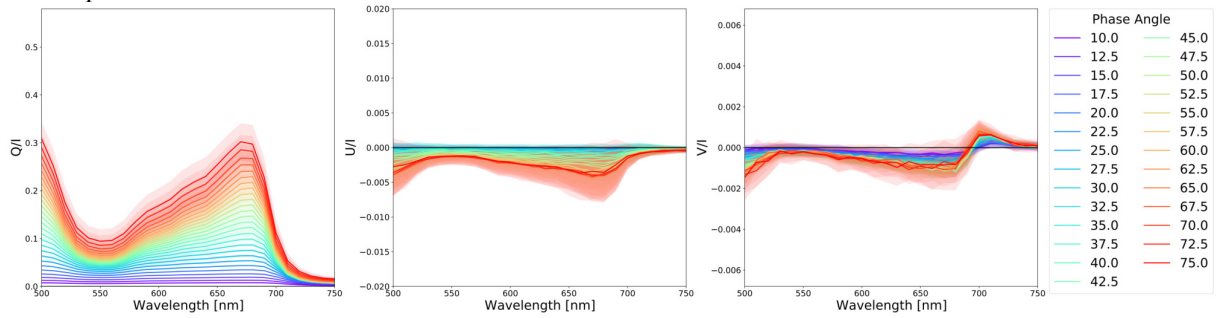
Quercus robur



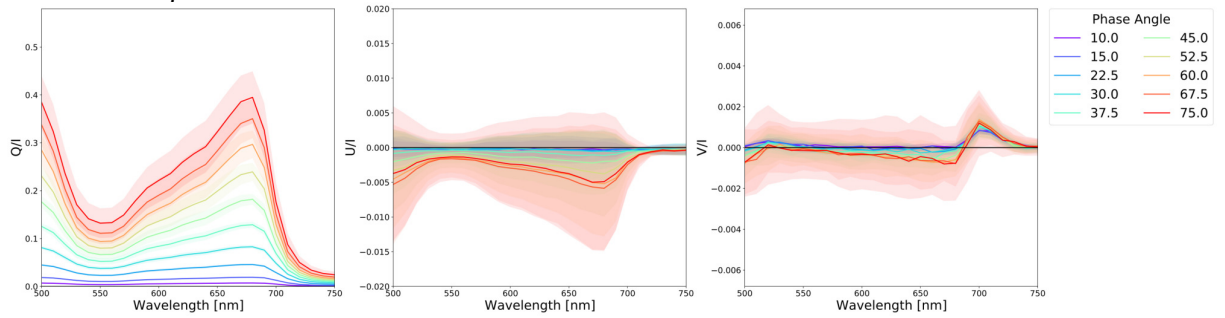
Reynoutria japonica



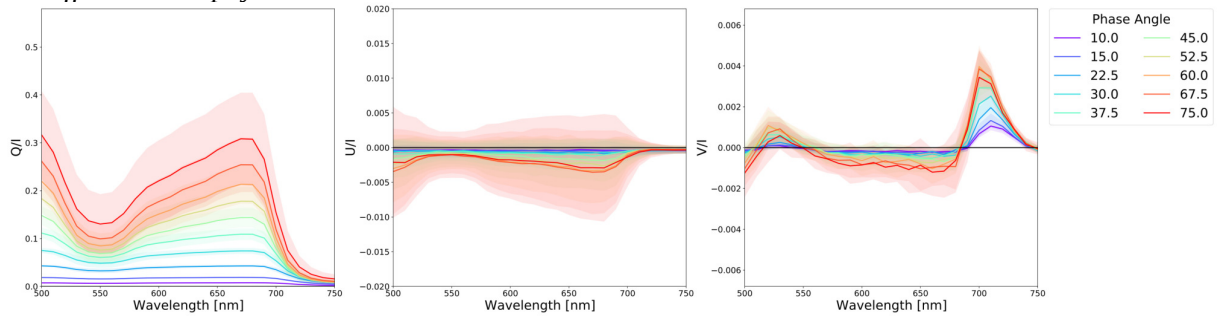
Rosa sp.



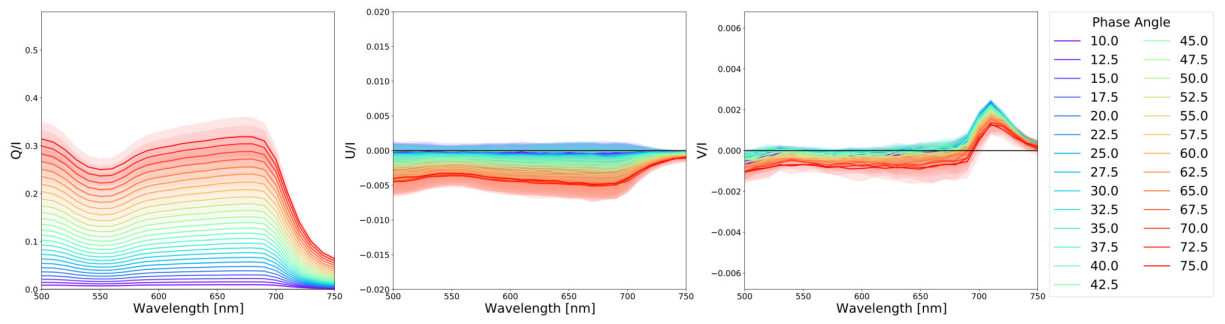
Rumex obtusifolius



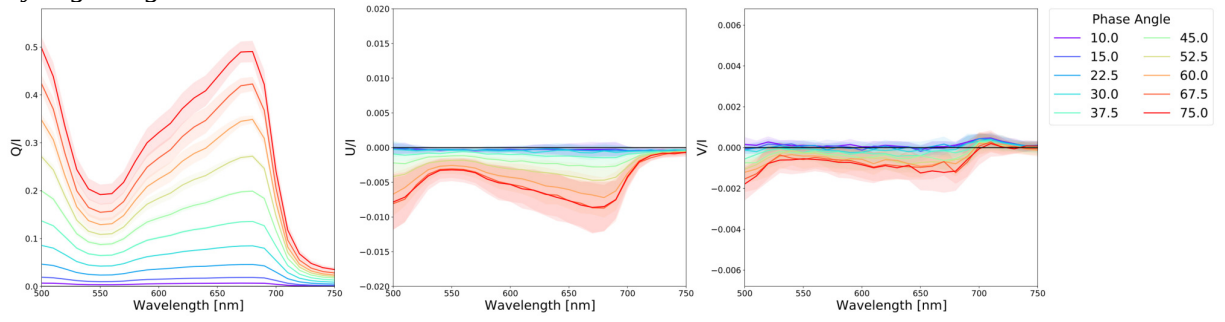
Schefflera actinophylla



Scindapsus pictus



Syringa vulgaris



Viola odorata

